Nanowire heterostructures

One-Dimensional Heterostructures of Single-Walled Carbon Nanotubes and CdSe Nanowires

*Nan Fu, Zhen Li, Anton Myalitsin, Matteo Scolari, R. Thomas Weitz, Marko Burghard, and Alf Mews**

Hybrid nanostructures from different nanomaterials are attracting increasing attention due to the possibility of tuning their chemical, electronic, and optical properties over a wide range. So far, research has focused on the combination of one-dimensional (1D) systems such as nanotubes and nanowires (NWs) with zero-dimensional (0D) objects such as semiconductor or metal nanoparticles.[1–6] In the field of carbon nanotubes (CNTs), the anchoring of different types of metal, semiconductor, and insulator nanoparticles has enabled numerous fundamental and application-related studies. For instance, CNTs bearing appropriate metal particles have been successfully employed in gas sensors[7,8] and fuel cells,[9,10] and closely attached noble metal nanoparticles have been shown to strongly enhance the Raman response of the underlying CNTs.[11–13] Moreover, CNTs modified by anchoring semiconductor nanoparticles via linker molecules[14–23] or direct semiconductor growth by colloidal routes[24] have found applications in photo-induced charge separation and transfer[21,22] as well as fluorescence visualization.[20] Likewise, different kinds of semiconductor nanowires, which are accessible through a range of methods including chemical vapor deposition (CVD),[25,26] thermal evaporation,[27] laser ablation,[28] and the solution–liquid–solid (SLS) process,[29–31] have been utilized as a platform for the assembly of nanowire–nanoparticle hybrids. Such structures are promising for applications in field-effect devices[32] and photocatalysis.[33–36]

Despite the recent progress made on hybrid nanostructures composed of 1D and 0D systems, only a few studies have been performed on hybrids comprising different 1D systems. Here we report on the synthesis as well as structural and optical characterization of a novel 1D heterostructure comprising single-walled carbon nanotubes (CNTs) and CdSe nanowires attached to the tube walls. Their synthesis involves two subsequent steps, namely i) the electrodeposition of Bi nanoparticles onto well-separated CNTs[37] and ii) the growth of CdSe nanowires using the attached Bi nanoparticles as catalysts.[38,39] The growth of CdSe nanowires in the second step is mediated by the Bi particles' low melting point combined with their dissolving capability for cadmium and selenium precursors.[29,30,40,41] The intriguing optical and electrical properties of the two types of nanowires, along with the unique properties of Bi nanoparticles such as a high figure of merit (ZT)[42–44] and the occurrence of a semimetal–semiconductor transition (for particle sizes below 50 nm),[45,46] render the CdSe NW–CNT hybrids promising building blocks for thermoelectric devices[44,47] and solar cells.[22]

The CNTs were grown directly on SiO_2/Si substrates by CVD using $FeCl_3$ as a catalyst.[48] After depositing photolithographically patterned Ti/Au electrodes, the substrates were placed inside an electrochemical cell, where Bi was electrodeposited onto the tubes through reduction of Bi-III ions (see Supporting Information). Metal electrodeposition on CNTs is a well-established method, although it has mostly been applied to noble metals such as Ag, Au, and Pt.[11,13,37,49] Bismuth is distinguished from these metals by being a semimetal with a low melting point (271.3 °C for bulk material),[50,51] which requires different electrodeposition conditions. In particular, its compounds such as $BiCl_3$ are readily hydrolyzed in water, yielding insoluble BiClO. Consequently, a low pH-value and exclusion of oxygen are required to revert this reaction ($BiClO + 2HCl \rightarrow BiCl_3 + H_2O$). From the atomic force microscopy (AFM) images and particle size histograms of Figure 1 it can be seen that the average size of the electrochemically deposited Bi particles attached to the CNTs is in the range of 5–10 nm. However, it can also be seen that the diameter distribution of the Bi particles depends sensitively on the $BiCl_3$ concentration, the deposition potential, and also on the deposition time. As a general trend, an increase in deposition time (Figure 1b), application of a more negative potential (Figure 1c), as well as the use of a higher $BiCl_3$ concentration (Figure 1d) resulted in a larger size of the Bi particles. The observed sensitive dependence of particle size on the electrodeposition conditions is similar to the case of noble metals on CNTs.[37,49]

The subsequent growth of CdSe nanowires from the electrodeposited Bi nanoparticles was carried out using an SLS process, similar to a previous protocol where the Bi particles were prepared by heating a flat Si substrate with a thin layer of thermally grown Bi layer.[38] However, while the diameter of the Bi particles obtained from the Bi layer were in the range of 50–100 nm, the electrodeposited Bi particles in this

[*] Prof. A. Mews, Dr. N. Fu, Dr. Z. Li, A. Myalitsin, Dr. M. Scolari
University of Hamburg
Grindelallee 117, 20146 Hamburg (Germany)
E-mail: alf.mews@chemie.uni-hamburg.de
Dr. R. T. Weitz, Dr. M. Burghard
Max-Planck-Institut für Festkörperforschung
Heisenbergstrasse 1, 70569 Stuttgart (Germany)

Supporting Information is available on the WWW under http://www.small-journal.com or from the author.

DOI: 10.1002/smll.200901366

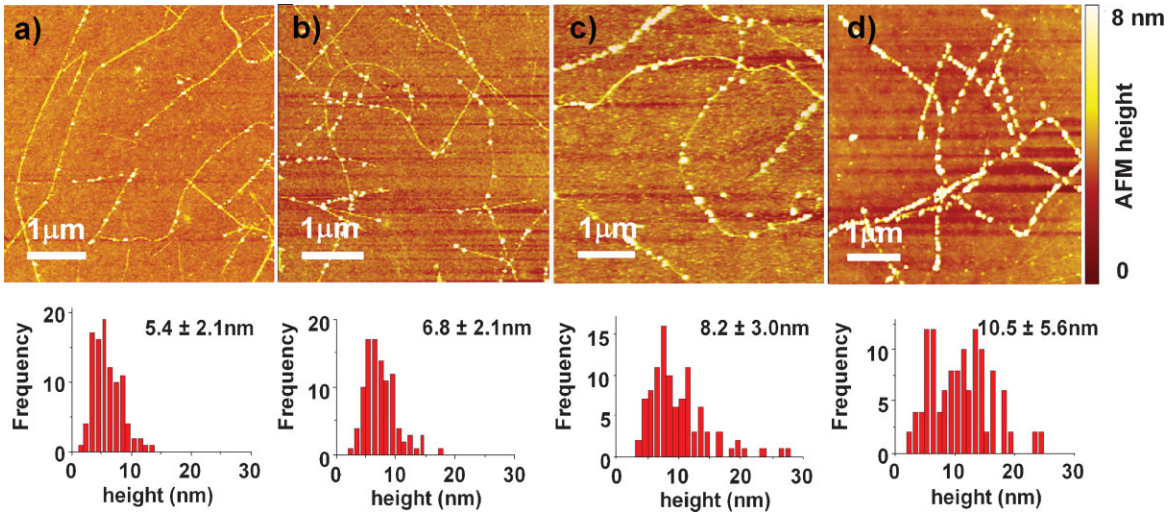

Figure 1. AFM images of CNTs with attached Bi nanoparticles and corresponding Bi particle height distributions obtained after different electrochemical conditions: a) 0.05 mM $BiCl_3$, −1.1 V for 5 s; b) 0.05 mM $BiCl_3$, −1.0 V for 8 s; c) 0.05 mM $BiCl_3$, −1.1 V for 8 s; d) 0.1 mM $BiCl_3$, −1.1 V for 8 s. The diameter, as well as the density, of the Bi nanoparticles on the CNTs increases from (a) to (d).

work are of considerably smaller size. This enables the growth of much thinner CdSe nanowires with a diameter in the strong quantum-confinement regime (<10 nm in diameter). To obtain a high yield of nanowires, it proved vital to keep the concentration of Cd and Se precursors in close proximity to the Bi@CNT particles very high. To this end, the cadmium and selenium precursor stock solution was loaded directly on the substrate with the CNT–Bi structures. For nanowire growth, the substrate was then immersed under argon protection into the tri-n-octylphosphine oxide (TOPO) solution kept at a reaction temperature of 150–300 °C.

Figure 2a–c shows AFM images of the same substrate area at different nanowire growth stages. In each image, the circles (1–3) and square (4) indicate the same position before (Figure 2a) and after electrodeposition (Figure 2b), as well as after nanowire growth (Figure 2c). The Bi-particles predominantly remained at the same location, suggesting a "base growth" mechanism for the CdSe wire growth, in contrast to the growth of homogeneous branchlike nanowires.[39] However, it is noteworthy that the diameter of these particular CdSe nanowires is approximately 8 nm, which significantly exceeds the size of the original Bi nanoparticle seeds (≈3 nm) in Figure 2b. However, a closer inspection evidences that the size of the Bi nanoparticles has increased from 3 to 14 nm during CdSe nanowires growth, that is, in comparing their AFM heights in Figures 1b and 2c.

In general, the growth of the Bi nanocatalysts during the SLS growth of CdSe nanowires has also been observed in homogeneous solutions with dissolved Bi particles.[52] Here it has been concluded that the liquid Bi nanodroplets fuse upon collision in the hot reaction solution. While such a mechanism appears reasonable for solution reactions with mobile reactants, in the present work the Bi particles are expected to be fixed on the CNT surface. However, in control experiments involving exposure of the Bi@CNTs structures to a hot TOPO solution, but without addition of Cd/Se precursors, we found that at temperatures above 200 °C the particles became slightly mobile and change their position by less than 100 nm (see Supporting Information). When the temperature was raised above 300 °C the particles detached completely from the CNTs and could not be located anymore by AFM. Based on these observations, we tentatively ascribe the Bi particle size increase during the CdSe nanowire growth to the fusion of small Bi aggregates, as exemplified by the squares in Figure 2b and c, respectively. In addition we found that the Bi particle growth is more pronounced during CdSe wire growth, as compared to

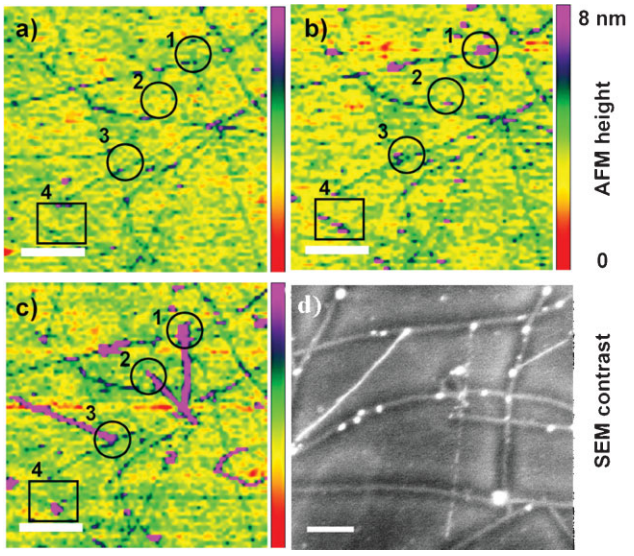

Figure 2. a-c) AFM images of the same sample area at different stages of preparation. The circles (1–3) and square (4) mark the same positions on the sample surface. CNTs from an identical area of the substrate after different stages of modification (scale bar is 500 nm). a) CNTs grown by CVD with an average AFM height of 1–2 nm; b) CNTs decorated with Bi nanoparticles by ECM. The height of the Bi particle at position (3) is 3 nm and several Bi particles can are observed at position (4). c) Successive growth of CdSe nanowires with a diameter of about 8 nm from Bi particle (3), which increased in height from 3 to 14 nm upon CdSe wire growth. Bi particle aggregation can be observed at area (4). d) SEM image (scale bar is 200 nm) of a different area on the same substrate, where the CNTs, Bi NCs, and CdSe NWs can clearly be distinguished.

heat treatment without the addition of CdSe precursors. Hence, we further argue that the ''mobility'' of the Bi species is enhanced upon loading with Cd and Se because of melting point reduction. For example, even in bulk materials the eutectic mixture of 4% CdSe in Bi reduces the melting point of Bi from 271 °C to 264 °C.[53] For small Bi particles the melting point is even lower and values of less than 100 °C have been reported for particle sizes below 1 nm,[54] while virtually no data exists for nanoscopic eutectic mixtures. However, highly mobile and reactive Cd–Bi–Se intermediates might be formed during the synthesis, which simultaneously accelerate both the Bi particle growth and also the CdSe nanowires formation.

At lower temperatures, the reduced Bi mobility and the corresponding possibility to keep the Bi particles small could be exploited to grow thinner CdSe nanowires. For example, at a reaction temperature of 200 °C, the average size of the Bi particles increased from originally 9 nm to 15 nm after CdSe nanowire growth, with a mean diameter of the resulting nanowires of 12 nm. Even at a reaction temperature of 150 °C CdSe nanowires were formed, albeit only from less than 15% of the Bi particles whose diameter is below 6 nm. Particles with a larger diameter did not show any catalytic activity at all, in agreement with the size-dependent melting point of Bi nanoparticles.[54] With rising reaction temperature, the nanowire yield gradually increased, along with a broadening of the diameter distribution of the Bi nanoparticles and CdSe nanowires (see Supporting Information). Specifically, while a yield of about 20% was obtained at 180 °C, it increased to 50% at 200 °C, and more than 80% at 250 °C. At the same time, the Bi particles became increasingly mobile, until at 250 °C they almost completely detached from the CNTs.

For the growth of longer CdSe nanowires, we employed a multiple growth technique similar to that in Reference [38]. In this reaction sequence, the substrate was removed from the liquid TOPO solution under Ar protection after the first growth step at 180 °C, and an additional drop of precursor solution was loaded on the sample surface. Finally, the sample was again immersed into the solution but now at a higher temperature (200 °C). In this manner, the length of nanowires could be notably increased from 0.8 ± 0.3 μm after the first growth step to 2.3 ± 1.3 μm after the second step (see also Figure 2). It should be emphasized that, if the sample was completely removed from the reaction flask and exposed to air, no further growth could be observed, most likely because of oxidative deactivation of the Bi particles.

The optical properties of the CNT–Bi–CdSe structures were studied using combined Raman and fluorescence microscopy and spectroscopy of individual nanoassemblies. The detection of Raman signals allows imaging and localizing of CNTs on the substrate, as well as determination of the structure and electronic properties of individual nanotubes.[55] Semiconductor nanowires, on the other hand, can be localized by their fluorescence, with the fluorescence wavelength being characteristic of their diameter and fluorescence intensity fluctuations, providing a measure for the charge-carrier dynamics.[56,57] Figure 3a displays an AFM image of a typical sample surface with CNT–Bi–CdSe structures, where the CdSe nanowires have been grown by the multiple injection method described above. It can be seen that several CdSe

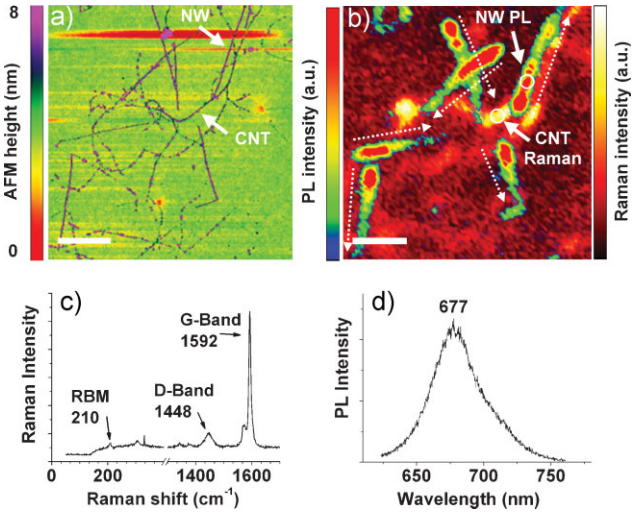

Figure 3. a) AFM image (1-μm scale bar) of CNT–NW heterostructures, with marked CdSe nanowire and CNTs; b) overlay of a Raman image of the CNTs and a fluorescence image of the CdSe nanowires (1-μm scale bar) from the same area as in (a); dotted arrows indicate the growth direction of nanowires. c) Raman spectrum of the CNT indicated by the arrow in (a) and (b); d) fluorescence spectrum of the CdSe nanowire indicated by the arrow in (a) and (b).

nanowires are still attached to the CNTs via Bi particles, even though the growth was performed through in two steps. In Figure 3b, an overlay of a fluorescence image of the CdSe nanowires (red) and a Raman G-band image of the CNTs (yellow) is depicted. The Raman intensity is strongly dependent on the resonance conditions, that is, only those tubes where the absorbed or scattered light is in resonance with the excitation energy can be observed in the image.[58] By contrast, the fluorescence can be detected from every nanowire, although its intensity changes along the wire axis.

Most nanowires displayed a stronger intensity at the thinner part close to the Bi catalyst, as exemplified by another set of nanowires in Figure 4. The scanning electron microscopy (SEM) picture in Figure 4a shows two nanowires whose diameters increase along the wire axis. For the left-hand nanowire the SEM image as well as the AFM image (not shown) revealed a diameter of 5 nm close to the Bi catalyst, which increases to about 9 nm at the end of the wire. The corresponding fluorescence image in Figure 4b evidences that the fluorescence intensity is considerably higher at the thinner nanowire section. Concomitantly, the emission wavelength is shifted from 655 to 690 nm (Figure 4c), in agreement with the diameter dependence of fluorescence of CdSe-NWs grown from dispersed Bi-particles in solution.[40]

To explain the origin of the inhomogeneous diameter of the NWs and the enhanced fluorescence of the thinner nanowire sections, the specific reaction conditions in our synthesis procedure may play an important role. In particular, since the Bi particles are located at the CNT surface the diameter might increase through fusion only during the first stage of reaction. After this initial stage no further Bi precursor is delivered from solution, and the Bi might partially dissolve into the CdSe nanowire and thus shrink during further growth. However,

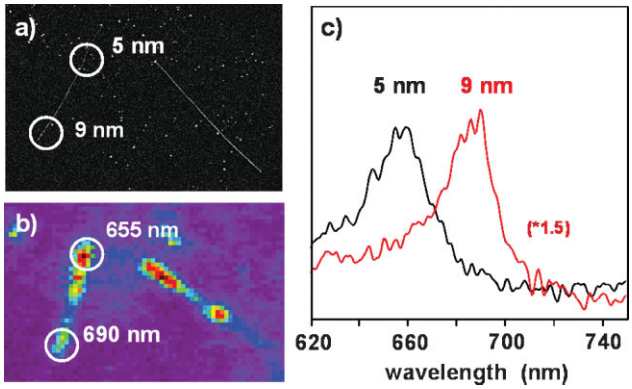

Figure 4. Correlation of morphology, fluorescence intensity, and fluorescence spectra of individual CdSe nanowires. a) SEM image of two CdSe nanowires, where the diameter is gradually increasing away from the Bi catalyst. b) Fluorescence image ($\lambda_{ex} = 514$ nm) showing a higher fluorescence intensity at the thinner part of the NW close to the Bi particle. c) Fluorescence spectra taken at the positions marked in (a) and (b). The fluorescence wavelength shifts to higher energies for smaller parts of the NWs according to size quantization effects.

since the amount of Bi dissolved in the CdSe nanowires is expected to be very low it cannot be detected within the accuracy of energy-dispersive X-ray spectroscopy (EDAX).[53] Nevertheless, it may well be that smaller amounts of Bi below the detection limit of the EDAX measurements are doped into the CdSe nanowires, which leads to a gradual decrease of the Bi nanocatalyst volume and hence a gradual decrease of the CdSe nanowires during the growth process. A similar mechanism was suggested for silicon NWs grown from gold catalysts by the vapor–liquid–solid (VLS) mechanism.[59] Moreover, a recent theoretical study has predicted that the impurity concentration of the catalyst material inside the nanowire decreases with the wire diameter.[60] Such dependence may also explain the low fluorescence intensity of the CdSe nanowires in general (QY < 1%),[61] as well as the fluorescence intensity modulation along the wires. Since Bi impurities will lead to an n-type doping of the CdSe nanowires, the excess charge carriers could quench the NW fluorescence in an Auger-like process, a mechanism that has been proposed for the quenching of CdSe nanocrystals.[62] In addition, if the relative amount of Bi at thinner sections of the CdSe nanowire is indeed reduced, this might explain the increase of fluorescence at the thinner part of the nanowires. However, a more detailed analysis of the structure and chemical composition of the nanowires along with investigations of the fluorescence dynamics of individual nanowires are needed to test these assumptions.

In conclusion, we have shown that Bi particles electrodeposited onto CNTs are suitable catalysts for the subsequent growth of CdSe nanowires. The electrodeposition parameters allow control over the size and density of the Bi nanoparticles, and thus the density of CNT–CdSe nanowire branches. The SLS growth yields CdSe wires of controllable diameter in the range of 4 to 12 nm, and wire lengths of up to several micrometers can be reached using a multiple injection technique. The CNT–CdSe nanowire hybrids are of interest for fundamental studies of luminescence quenching in dependence of charge-carrier densities and current flow, as well as for applications in photoelectric or thermoelectric devices.

Experimental Section

Electrodeposition of Bi nanoparticles onto CNTs: Bismuth solution was prepared with 0.05 to 0.1 mM $BiCl_3$, 1 M HCl, 1 mM KCl as an electrolyte and 5 mM poly-(vinylpyridine) as a surfactant. Then the solution was purged with Ar for 20 minutes in order to get rid of dissolved oxygen. A potentiostat (HEKA Potentiostat galvanostat PG 310) was used to apply potential during the experiment, supplied with a tungsten needle as a working electrode, and silver and platinum wire as reference and counter electrodes, respectively. The as-prepared substrate with patterned electrodes and CNTs on surface was immersed into the bismuth solution in an electrochemical cell made of Teflon, where three electrodes are also immersed (see Supporting Information). Before applying potential, the tungsten working electrode was positioned through a microscope onto the patterned electrode on the substrate. During the electrochemical modification process, negative potentials from −0.9 V to −1.5 V with respect to the reference silver electrode were applied for 5 to 10 s on the working electrode, which was connected with CNTs on the substrate surface. Afterwards, the sample was taken out from the solution and rinsed by DI water.

Growth of CdSe nanowires using the attached Bi nanoparticles as catalyst: Firstly, Se powder was dissolved in trioctylphosphine (TOP) to prepare a 1 M Se–TOP solution as a stock solution in a glove box. A reaction flask containing about 3 g tri-n-octylphosphine oxide (TOPO) was evacuated for 30 minutes at 100 °C, then filled with Ar. Afterwards, 10 μL Se–TOP stock solution was loaded onto the substrate surface with the Bi-modified CNTs and then the substrate was immersed into the TOPO solution at growth temperature from 150 °C to 300 °C. Meanwhile, 10 μL of highly reactive dimethyl cadmium solution ($Cd(Me)_2$) was also injected (see Supporting Information). After 1 to 10 minutes, depending on the reaction temperature, the substrate was taken off the solution and rinsed with toluene to remove byproducts such as deposited CdSe nanoparticles. Alternatively, to avoid using the hazardous compound $Cd(Me)_2$, $Cd(CH_3(CH_2)_6COO)_2$ solution was prepared as a Cd precursor by dissolving CdO in octanoic acid $Cd(CH_3(CH_2)_6COO)_2$. During the reaction, a drop of $Cd(CH_3(CH_2)_6COO)_2$-TOP solution (1 M) was loaded directly onto a substrate surface together with a drop of Se-TOP (1 M) in the flask under the protection of Ar, keeping the ratio of Cd:Se as 1:1. At the reaction temperature, the substrate was immersed into the TOPO solution and the growth of CdSe nanowires took place from Bi nanoparticles on the substrate.

NW-CNT heterostructure imaging: NW-CNT heterostructure imaging: After electrochemical deposition of Bi nanoparticles on CNTs as well as CdSe nanowire growth, sample surfaces were characterized by a NanoScope IV Multimode atom force microscope from Veeco Digital Instruments in tapping mode. By adjusting the colour table of the images, nanowires could be distinguished from CNTs due to the large difference of their diameters. Moreover, combined Raman and fluorescence microscopy and spectroscopy of individual nanostructures were obtained by our home-made single-molecule laser spectrometer. In our experiments, the complete fluorescence emission above 520 nm was selected by an optical filter in front of the detector to acquire a fluorescence image of nanowires by scanning the sample through the focus of the laser spot. Likewise, the G-band

of the CNTs, which is shifted by 1592 cm^{-1} with respect to the laser excitation energy (514 nm), was filtered by a monochromator to image the CNTs, as shown in Figures 3 and 5. Meanwhile, Raman and fluorescence spectra of individual CNTs and nanowires could also be obtained by the spectrometer.

Keywords:
electrochemical modification · carbon nanotubes · heterostructures · hybrid nanostructures · semiconductor nanowires

[1] A. J. Mieszawska, R. Jalilian, G. U. Sumanasekera, F. P. Zamborini, *Small* **2007**, *3*, 722–756.
[2] R. H. Baughman, A. A. Zakhidov, W. A. de Heer, *Science* **2002**, *297*, 787–792.
[3] S. J. Tans, A. R. M. Verschueren, C. Dekker, *Nature* **1998**, *393*, 49–52.
[4] H. Dai, *Surface Science* **2002**, *500*, 218–241.
[5] K. Balasubramanian, M. Burghard, K. Kern, M. Scolari, A. Mews, *Nano Lett.* **2005**, *5*, 507–510.
[6] X. H. Peng, J. Y. Chen, J. A. Misewich, S. S. Wong, *Chem. Soc. Rev.* **2009**, *38*, 1076–1098.
[7] Q. Zhao, M. B. Nardelli, W. Lu, J. Bernholc, *Nano Lett.* **2005**, *5*, 847–851.
[8] E. Bekyarova, M. Davis, T. Burch, M. E. Itkis, B. Zhao, S. Sunshine, R. C. Haddon, *J. Phys. Chem. B* **2004**, *108*, 19717–19720.
[9] G. Girishkumar, K. Vinodgopal, P. V. Kamat, *J. Phys. Chem. B* **2004**, *108*, 19960–19966.
[10] C. H. Yen, K. Shimizu, Y–. Y. Lin, F. Bailey, I. F. Cheng, C. M. Wai, *Energy & Fuels* **2007**, *21*, 2268–2271.
[11] M. Burghard, A. Maroto, K. Balasubramanian, T. Assmus, A. Forment–Aliaga, E. J. H. Lee, R. T. Weitz, M. Scolari, N. Fu, A. Mews, K. Kern, *Phys. Stat. Sol.* **2007**, *244*, 4021–4025.
[12] M. Scolari, A. Mews, N. Fu, A. Myalitsin, T. Assmus, K. Balasubramanian, M. Burghard, K. Kern, *J. Phys. Chem. C* **2008**, *112*, 391–396.
[13] T. Assmus, K. Balasubramanian, M. Burghard, K. Kern, M. Scolari, N. Fu, A. Myalitsin, A. Mews, *Appl. Phys. Lett.* **2007**, *90*, 173109.
[14] X. Li, Y. Liu, L. Fu, L. Cao, D. Wei, Y. Wang, *Adv. Funct. Mater.* **2006**, *16*, 2431–2437.
[15] V. Georgakilas, V. Tzitzios, D. Gournis, D. Petridis, *Chem. Mater.* **2005**, *17*, 1613–1617.
[16] S. Banerjee, S. S. Wong, *J. Am. Chem. Soc.* **2003**, *125*, 10342–10350.
[17] S. Ravindran, S. Chaudhary, B. Colburn, M. Ozkan, C. S. Ozkan, *Nano Lett.* **2003**, *3*, 447–453.
[18] J. M. Haremza, M. A. Hahn, T. D. Krauss, S. Chen, J. Calcines, *Nano Lett.* **2002**, *2*, 1253–1258.
[19] S. Banerjee, S. S. Wong, *Nano Lett.* **2002**, *2*, 195–200.
[20] S. Chaudhary, J. H. Kim, K. V. Singh, M. Ozkan, *Nano Lett.* **2004**, *4*, 2415–2419.
[21] D. M. Guldi, G. M. A. Rahman, V. Sgobba, N. A. Kotov, D. Bonifazi, M. Prato, *J. Am. Chem. Soc.* **2006**, *128*, 2315–2323.
[22] L. Hu, Y. L. Zhao, K. Ryu, C. Zhou, J. F. Stoddart, G. Grüner, *Adv. Mater.* **2008**, *20*, 939–946.
[23] C. Engtrakul, Y. H. Kim, J. M. Nedeljkovic, S. P. Ahrenkiel, K. E. H. Gilbert, J. L. Alleman, S. B. Zhang, O. I. Micic, A. J. Nozik, M. J. Heben, *J. Phys. Chem. B* **2006**, *110*, 25153–25157.
[24] B. H. Juarez, C. Klinke, A. Kornowski, H. Weller, *Nano Lett.* **2007**, *7*, 3564–3568.
[25] J.-P. Ge, J. Wang, H.-X. Zhang, Y.-D. Li, *Chem. Eur. J.* **2004**, *10*, 3525–3530.
[26] C. X. Shan, Z. Liu, S. K. Hark, *Appl. Phys. Lett.* **2007**, *90*, 193123.
[27] C. Ma, Y. Ding, D. Moore, X. Wang, Z. L. Wang, *J. Am. Chem. Soc.* **2004**, *126*, 708–709.
[28] A. M. Morales, C. M. Lieber, *Science* **1998**, *279*, 208–211.
[29] T. J. Trentler, K. M. Hickman, S. C. Goel, A. M. Viano, P. C. Gibbons, W. E. Buhro, *Science* **1995**, *270*, 1791–1794.
[30] Y. Xia, P. Yang, Y. Sun, Y. Wu, B. Mayers, B. Gates, Y. Yin, F. Kim, H. Yan, *Adv. Mater.* **2003**, *15*, 353–389.
[31] N. Pradhan, H. Xu, X. Peng, *Nano lett.* **2006**, *6*, 720–724.
[32] Y. Huang, X. Duan, Y. Cui, L. J. Lauhon, K–. H. Kim, C. M. Lieber, *Science* **2001**, *294*, 1313–1317.
[33] T. Mokari, C. G. Sztrum, A. Salant, E. Rabani, U. Banin, *Nat. Mater.* **2005**, *4*, 855–863.
[34] A. Salant, E. Amitay-Sadovsky, U. Banin, *J. Am. Chem. Soc.* **2006**, *128*, 10006–10007.
[35] A. E. Saunders, I. Popov, U. Banin, *J. Phys. Chem. B* **2006**, *110*, 25421–25429.
[36] R. Costi, A. E. Saunders, E. Elmalem, A. Salant, U. Banin, *Nano Lett.* **2008**, *8*, 637–641.
[37] T. M. Day, P. R. Unwin, N. R. Wilson, J. V. Macpherson, *J. Am. Chem. Soc.* **2005**, *127*, 10639–10647.
[38] L. Ouyang, K. N. Maher, C. L. Yu, J. McCarty, H. Park, *J. Am. Chem. Soc.* **2007**, *129*, 133–138.
[39] A. Dong, R. Tang, W. E. Buhro, *J. Am. Chem. Soc.* **2007**, *129*, 12254–12262.
[40] H. Yu, J. Li, R. A. Loomis, P. C. Gibbons, L. W. Wang, W. E. Buhro, *J. Am. Chem. Soc.* **2003**, *125*, 16168–16169.
[41] J. W. Grebinski, K. L. Hull, J. Zhang, T. H. Kosel, M. Kuno, *Chem. Mater.* **2004**, *16*, 5260–5272.
[42] L. D. Hicks, M. S. Dresselhaus, *Phys. Rev. B* **1993**, *47*, 12727–12731.
[43] L. D. Hicks, T. C. Harman, M. S. Dresselhaus, *Appl. Phys. Lett.* **1993**, *63*, 3230–3232.
[44] T. C. Harman, P. J. Taylor, M. P. Walsh, B. E. LaForge, *Science* **2002**, *297*, 2229–2232.
[45] X. Sun, Z. Zhang, M. S. Dresselhaus, *Appl. Phys. Lett.* **1999**, *74*, 4005–4007.
[46] M. R. Black, Y. M. Lin, S. B. Cronin, O. Rabin, M. S. Dresselhaus, *Phys. Rev. B* **2002**, *65*, 195417.
[47] A. Majumdar, *Science* **2004**, *303*, 777–778.
[48] H. C. Choi, S. Kundaria, D. Wang, A. Javey, Q. Wang, M. Rolandi, H. Dai, *Nano Lett.* **2003**, *3*, 157–161.
[49] B. M. Quinn, C. Dekker, S. G. Lemay, *J. Am. Chem. Soc.* **2005**, *127*, 6146–6147.
[50] Y. W. Wang, B. H. Hong, K. S. Kim, *J. Phys. Chem. B* **2005**, *109*, 7067–7072.
[51] E. A. Olson, M. Y. Efremov, M. Zhang, Z. Zhang, L. H. Allen, *J. Appl. Phys.* **2005**, *97*, 034304.
[52] Z. Li, A. Kornowski, A. Myalitsin, A. Mews, *Small* **2008**, *4*, 1698–1702.
[53] P. Villars, A. Prince, H. Okamoto, in *Handbook of Ternary Alloy Phase Diagrams*, Vol. *5*, Wiley, Weinheim, Germany **1995**.
[54] G. Kellermann, A. F. Craievich, *Phys. Rev. B* **2008**, *78*, 054106.
[55] A. Mews, F. Koberling, T. Basche, G. Philipp, G. S. Duesberg, S. Roth, M. Burghard, *Adv. Mater.* **2000**, *12*, 1210–1214.
[56] J. J. Glennon, r, Tang, W. E. Buhro, A. R. Loomis, *Nano Lett.* **2007**, *7*, 3290–3295.
[57] V. V. Protasenko, K. L. Hull, M. Kuno, *Adv. Mater.* **2005**, *17*, 2942–2949.
[58] S. Reich, C. Thomsen, J. Maultzsch, *Carbon Nanotubes*, Wiley, Weinheim, Germany **2004**.
[59] J. B. Hannon, S. Kodambaka, F. M. Ross, R. M. Tromp, *Nature* **2006**, *440*, 69–71.
[60] E. J. Schwalbach, P. W. Voorhees, *Nano Lett.* **2008**, *8*, 3739–3745.
[61] M. Kuno, *Phys. Chem. Chem. Phys.* **2008**, *10*, 620–639.
[62] A. L. Efros, M. Rosen, *Phys. Rev. Lett.* **1997**, *78*, 1110–1113.

Received: July 27, 2009
Revised: September 30, 2009
Published online: December 21, 2009

